Available online at www.sciencedirect.com

ScienceDirect

www.elsevier.com/locate/jes

JES JOURNAL OF ENVIRONMENTAL SCIENCES

www.jesc.ac.cn

Adsorption of Ca^{2+} on single layer graphene oxide

Amalia Terracciano[1], *Jianfeng Zhang*[2], *Christos Christodoulatos*[1], *Fengchang Wu*[3], *Xiaoguang Meng*[1,*]

1. *Center for Environmental Systems, Stevens Institute of Technology, Hoboken, NJ 07030, USA*
2. *School of Environmental and Municipal Engineering, Xi'an University of Architecture and Technology, Xi'an 710055, China*
3. *State Key Laboratory of Environmental Criteria and Risk Assessment, Chinese Research Academy of Environmental Sciences, Beijing 100012, China*

ARTICLE INFO

Article history:
Received 1 September 2016
Revised 11 January 2017
Accepted 12 January 2017
Available online 26 January 2017

Keywords:
Graphene oxide
Calcium adsorption
Raman spectra
Colloidal stability

ABSTRACT

Graphene oxide (GO) holds great promise for a broad array of applications in many fields, but also poses serious potential risks to human health and the environment. In this study, the adsorptive properties of GO toward Ca^{2+} and Na^{+} were investigated using batch adsorption experiments, zeta potential measurements, and spectroscopic analysis. When pH increased from 4 to 9, Ca^{2+} adsorption by GO and the zeta potential of GO increased significantly. Raman spectra suggest that Ca^{2+} was strongly adsorbed on the GO *via* –$COOCa^{+}$ formation. On the other hand, Na^{+} was adsorbed into the electrical diffuse layer as an inert counterion to increase the diffuse layer zeta potential. While the GO suspension became unstable with increasing pH from 4 to 10 in the presence of Ca^{2+}, it was more stable at higher pH in the NaCl solution. The findings of this research provide insights in the adsorption of Ca^{2+} on GO and fundamental basis for prediction of its effect on the colloidal stability of GO in the environment.

Introduction

Nanomaterials have attracted great attention and research interest due to their large specific surface area and abundant active groups. Among these, graphene and its derivatives have been in the spotlight in recent years. Graphene is a two-dimensional nanomaterial with one to ten layers of sp^2-hybridized carbon atoms arranged in six-membered rings, that has attracted tremendous attention due to its high mechanical strength (125 GPa fracture strength and 1100 GPa Young's modulus) (Lee et al., 2008), large specific surface area (theoretical value of 2600 m^2/g) (Rao et al., 2009) and exceptionally high electronic and thermal conductivity (200,000 $cm^2/(V{\cdot}sec)$) and approximately (5000 W/(m·K), respectively) (Balandin et al., 2008; Park and Ruoff, 2009) as well as many other remarkable properties. Graphene oxide (GO), as part of the graphene-based nanomaterials family (GNFs), has hexagonal carbon rings similar to those in graphene, but with many oxygen-containing functional groups, such as carboxyl (–COOH), hydroxyl (–OH), and epoxy (–O–) groups, at the edges and on the face of the GO nanosheets (Lerf et al., 1998; Lee et al., 2010), which can be differentially functionalized (Stankovich et al., 2006; Niyogi et al., 2006). The potential applications of GO and its functionalized derivatives include optoelectronics, biodevices, drug delivery systems and reinforced composites (Xu et al., 2009; Dreyer et al., 2010).

Although the applications of GO are exciting (Singh et al., 2011a), it may cause significant pathological effects for the

* *Corresponding author*. E-mail: xmeng@stevens.edu (Xiaoguang Meng).

http://dx.doi.org/10.1016/j.jes.2017.01.008
1001-0742/

environment and human health. In particular, GO nanoparticles can cause thrombus (Singh et al., 2011b), severe and persistent lung injury (Schinwald et al., 2012; Li et al., 2013) and damage to fetal growth, since their size allows them to cross the placenta (Arvidsson et al., 2013). Ecosystem equilibria could be seriously affected by the high antibacterial capacity and cytotoxicity of GO (Chen et al., 2012). The toxicity of GO to a series of common terrestrial plants (cabbage, tomato and red spinach) has also been reported (Zhao et al., 2014).

The effectiveness of GO has been demonstrated for removal of a wide range of environmental pollutants from wastewater. Several studies reported high adsorption capacity for GO toward different heavy metals such as Cu^{2+}, Cd^{2+}, Co^{2+}, $Ni^{2+}$and Pb^{2+} (Chandra et al., 2010; Li et al., 2011; Zhao et al., 2011a; Guo et al., 2012; Luo et al., 2012; Wang et al., 2013; Pei et al., 2013; Gu and Fein, 2015; Tan et al., 2015). The adsorption capacity was higher than for any other known material, which suggests promising prospects for applications in wastewater treatment and contaminant remediation (Yang et al., 2010; Zhao et al., 2011b; Chowdhury et al., 2013; Sitko et al., 2013). Since GO is highly hydrophilic and readily dispersed in water, studies have been conducted on the colloidal stability and mobility of GO nanoparticles in the aquatic environment, especially in the presence of electrolytes (Feriancikova and Xu, 2012; Chowdhury et al., 2014; Lanphere et al., 2014). Divalent and monovalent cations such as Ca^{2+} and Na^{+} are the most abundant cations, with a concentration range of about 1–135 mg/L (0.025–3.4 mmol/L) and 1–402 mg/L (0.043–17.5 mmol/L), in most freshwater (National Academy of Sciences, 1977; Hem, 1992; Lanphere et al., 2013). The results indicated that GO could be highly mobile in aquatic environments; however its mobility was significantly affected by the ionic strength (Stumm, 1992). The results obtained for divalent cation solutions indicated that Ca^{2+} can significantly influence the stability and mobility of GO in natural water. Although the effect of Ca^{2+} on the colloidal stability of GO has been generally attributed to electrostatic interaction, the nature of Ca^{2+} interactions with GO has not been studied.

In the present study, the mechanism of Ca^{2+} adsorption on GO was evaluated using adsorption tests and Raman spectroscopic analysis; results from zeta potential measurements also showed differences in the effect of Ca^{2+} adsorption on the zeta potential of the GO nanoparticles compared to Na^{+}.

1. Materials and methods

1.1. Materials

Single layer GO (SLGO) with purity >90%wt, XY dimensions (lateral) of 300–800 nm, thickness (Z dimension) of 0.7–1.2 nm and specific surface area (SSA) of 350–400 m^2/g was purchased from Cheap Tubes Inc. (Brattleboro, VT). The stock solution of GO was prepared by transferring 10 mg GO nanoparticles into 100 mL deionized (DI) water (nanopure water at >18.2 MΩ·cm at 25°C) and then dispersing the nanoparticles using a Sonic Dismembrator (Fisher Scientific, Model F550) at 25% power for 30 min. $MgCl_2$, NaCl, and $CaCl_2$ solutions, and 0.1 mol/L NaOH and HCl solutions used for pH adjustment, were prepared using ACS grade chemicals and DI water.

1.2. Batch adsorption experiments

A GO working solution was prepared by addition of the stock solution into DI water to reach a GO concentration of 20 mg/L. The working solution was dispersed with ultrasonication for 10 min before it was used in the experiments. Adsorption of Ca^{2+} and Na^{+} by GO nanoparticles was tested by mixing solutions containing 10 mg/L of GO and 1–4 mmol/L of Ca^{2+} or Na^{+} in 50 mL centrifuge tubes on a rotary mixer. After overnight mixing, the samples were centrifuged at 10,000 r/min for 30 min. The supernatant samples were collected and passed through a 0.22 μm syringe filter for analysis of soluble Ca^{2+} and Na^{+} concentrations using an inductively coupled plasma optical emission spectrometer (ICP–OES) (Varian Vista MPX). The amount of metal ions adsorbed on GO, q_e (mmol/g), was calculated from the difference between the initial concentration C_0 (mmol/L) in aqueous solution and the equilibrium concentration C_e (mmol/L) determined in solution after filtration: $q_e = (C_0 - C_e)V / m_{adsorbent}$, where V (L) is the volume of the suspension and $m_{adsorbent}$ (g) is the mass of GO.

1.3. Raman spectroscopy analysis

The Raman spectra were collected in high resolution mode with a dispersive Raman spectrometer (Thermo Nicolet Almega XR) equipped with a CCD detector, optical microscope, digital camera, and 780 nm laser line with a laser source power of 30 mW (50% power was applied in the analysis). The Raman band of a silicon wafer at 520 cm^{-1} was used to calibrate the spectrometer. All the measurements were conducted in the backscattering geometry. A 10× microscope objective was used, providing a laser spot size of 3.1 μm. The data acquisition time was 3 sec per scan, and 100 scans were used for each spectrum collection.

1.4. Effect of pH and cations on GO aggregation

The NaCl and $CaCl_2$ solutions were added into the GO working solution to reach the desired salt concentrations. An initial concentration of 10 mg/L of GO was used for all tests. The solution pH was adjusted to desired values using NaOH and HCl solutions at 0.1 mol/L. After 15 min of mixing, 2.5 mL samples were taken for measurement of the zeta potential and the hydrodynamic diameter (Dh) using a Nano ZetaSizer ZEN3600 (Malvern Instrument, UK).

2. Results and discussion

2.1. Adsorption of Ca^{2+} on GO

Batch adsorption experiments were carried out in order to assess the adsorption behavior of GO for Ca^{2+}. Adsorption kinetic results in Appendix A Fig. S1 showed that Ca^{2+} was

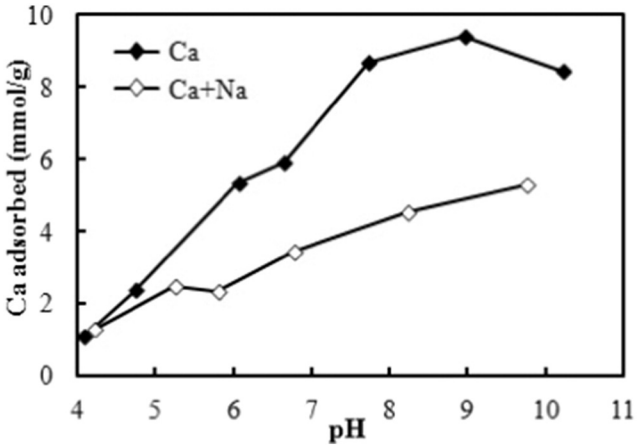

Fig. 1 – Adsorption of Ca^{2+} on GO as a function of pH. GO content = 10 mg/L, Ca^{2+} = 1 mmol/L and Na^{+} = 10 mmol/L in the binary component solution.

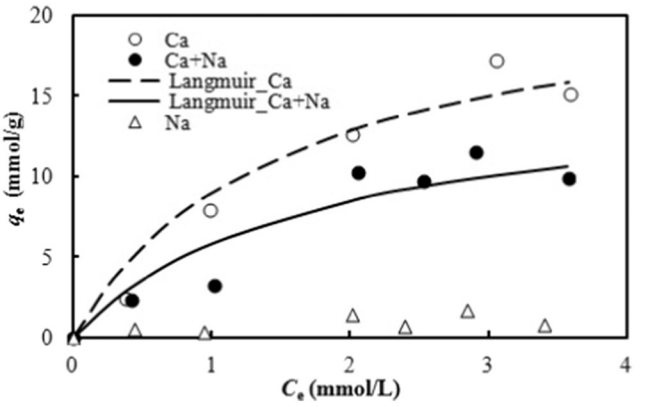

Fig. 2 – Adsorption isotherms of Ca^{2+} in solutions with and without 10 mmol/L Na^{+}, and adsorption of Na^{+}. GO content = 10 mg/L, pH = 7.0 ± 0.1.

adsorbed on GO rapidly and reached adsorption equilibrium in 15 min. A short time is required for the adsorption to reach equilibrium because the surface of the dispersed GO nanosheets is readily available to the adsorbates. Conventional adsorbents, such as granular activated carbon and activated alumina, have a long adsorption equilibrium time because of slow diffusion of adsorbates into the pores of the porous particles.

The adsorption of Ca^{2+} on GO was investigated at pH from 4 to 10 with and without addition of 10 mmol/L of Na^{+} in solution (Fig. 1). As shown, the adsorption of Ca^{2+} significantly increased with increasing pH, especially in the absence of Na^{+}. Adsorption of cations on metal oxide surfaces typically increases with increasing pH (Stumm, 1992). Calcium cations have been reported to bridge deprotonated carboxyl groups on organic matter and ionized OH groups (–O–) on mineral surfaces (*e.g.* goethite, aluminosilicates and kaolinite) through formation of complexes that involve electrostatic attraction between Ca^{2+} cations and negatively charged functional groups (Sposito, 2008).

Ionization of the oxygen-containing functional groups on the GO surface may play an important role in the adsorption of metal ions, which is favored at high pH. Adsorption isotherms were derived using adsorption data collected at pH 7 (Fig. 2) for both Ca^{2+} and Na^{+}. The amount of adsorbed Ca^{2+} increased with increasing Ca^{2+} concentration, with and without Na^{+} in solution, while no significant adsorption of Na^{+} was detected.

The adsorption isotherm data for Ca^{2+} and Ca^{2+} + Na^{+} were fitted using the Langmuir isotherm model. The Langmuir isotherm is expressed according to the following equation:

$$q_e = q_m K C_e / (1 + K C_e)$$

where, q_e (mmol/g) and q_m (mmol/g) are the amount of adsorbate on the adsorbent and the maximum adsorption capacity, respectively, K (L/mmol) is the Langmuir adsorption equilibrium constant, and C_e (mmol/L) is the equilibrium adsorbate concentration.

The Langmuir isotherm model assumes monolayer coverage of adsorbate over a homogenous adsorbent surface, and that the adsorption of each molecule onto the surface has the same activation energy of adsorption. The value of K indicates the strength or affinity of the adsorbent for the solute. The adsorption isotherms were well fitted by the Langmuir isotherm model (R^2[Ca^{2+}] = 0.891; r-square[Ca^{2+} + Na^{+}] =0.903) suggesting that adsorption of Ca^{2+} on GO occurs by monolayer coverage. The Langmuir model has been reported to be a suitable fit for adsorption of different heavy metals on GO (Yang et al., 2010). The amount of Ca^{2+} adsorbed on GO decreased in the presence of 10 mmol/L of Na^{+}, which was consistent with the results observed (Fig. 1). The q_{max} calculated from the Langmuir model was 15.3 mmol/g for Ca^{2+} + Na^{+} and 21.1 mmol/g in the presence of Ca^{2+} only. At present, there are no data available in the literature about the adsorption capacity of GO for Ca^{2+}; however Ca^{2+} was found the adsorbed on GO up to 50% of the original concentration in the pH range 7 to 8 following the same behavior of with Sr, Zn and Ni (Gu and Fein, 2015).

2.2. Spectroscopic characterization of GO

Raman spectroscopy is a standard nondestructive tool that has been widely used to characterize crystalline, nanocrystalline and amorphous carbon. It has been extensively used also to identify the electrostatic or chemical nature of adsorption mechanisms (Ramesha et al., 2011; Cañamares and Lombardi, 2015; Liu et al., 2016).

Fig. 3 shows the Raman spectra of GO in DI water and in NaCl and $CaCl_2$ solutions. The spectrum (Line a) of GO in DI water is similar to those reported in the literature (Ferrari and Robertson, 2000; Cañamares and Lombardi, 2015). The Raman spectra of GO, as part of the graphite based material family, is characterized by two prominent peaks at 1333 and 1594 cm^{-1}, corresponding to the D and G bands, respectively. The GO nanosheets can stack together in the suspension. The D band is associated with the order/disorder of the GO system; the peak arises from the carboxyl, hydroxyl and epoxy groups on the carbon skeleton. The G band indicates the stacking structure of GO as well as the stretching in the sp^2 sites (Das et al., 2000). The Raman spectra of GO in 2.0 mmol/L NaCl

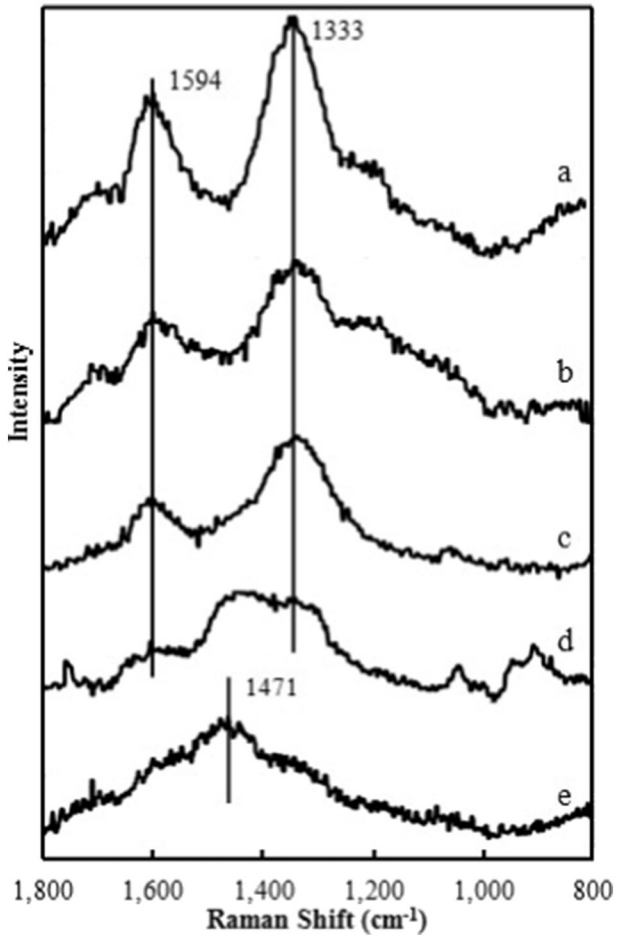

Fig. 3 – Raman spectra of (line a) GO, GO = 1000 mg/L; (line b) GO + 2.0 mmol/L Na^+; (line c) GO + 0.1 mmol/L Ca^{2+}; (line d) GO + 0.5 mmol/L Ca^{2+}; (e) GO + 1 mmol/L Ca^{2+}.

were similar to that of the GO in DI water. The results suggest that there were no strong bonding interactions between Na^+ and the surface functional groups, which is consistent with the small amount of Na^+ adsorbed by GO as shown in Fig. 2.

The Raman spectra of GO in 0.1 mmol/L $CaCl_2$ solutions were similar to that of the GO in DI water. However, when the concentration of Ca increases from 0.1 to 1 mmol/L, a significant change in intensity is showed for both the G and D band peaks. A new peak arose at 1471 cm^{-1} which may be attributed to a shift of the G band. The D band peak position is still visible with 1 mmol/L of $CaCl_2$, even with lower intensity if compared to the peak at 1470 cm^{-1}.

Both changes in intensity and shift of the G band peak for GO and graphene have been already reported (Das et al., 2000; Voggu et al., 2008); adsorption of dyes on Exfoliated Graphene Oxide (EGO) showed a small shift of the G band peak, which was attributed to charge transfer (Ramesha et al., 2011). Since the changes induced by Ca^{2+} adsorption on the GO Raman spectra are more dramatic, it is clear that Ca^{2+} has strong bonding interactions with the functional groups on GO, which are beyond electrostatic interaction only. It is known that Ca^{2+} forms complexes with carboxylic acids, such as m-hydroxybenzoic acid and 3,5-dihydroxybenzoic acid (Emara et al., 1984), and with carboxyl groups on humic and fulvic acids (Ouatmane et al., 1999). The Raman spectra, adsorption results, and previously reported complexation reactions of Ca^{2+} with carboxyl groups of organic compounds suggest that Ca^{2+} ions were strongly bound to carboxyl groups (–COOH) on GO to form inner-sphere complexes (*e.g.* –$COOCa^+$).

The possible formation of surface complexes neutralized the negative surface charges and increased the surface and zeta potential (Fig. 5). In contrast, Na^+ ions were electrostatically adsorbed in the diffuse layer to form outer-sphere surface complexes (*e.g.* –COO^-Na^+). The adsorbed counterions increased the zeta potential through charge screening, but could not affect the surface potential as shown by zeta potential measurements.

2.3. Effect of pH and cations concentration on GO aggregation

Fig. 4 shows the effect of pH on the zeta potential and size of GO nanoparticles in Na^+, Ca^{2+}+Na^+ and Mg^{2+} + Na^+ solutions. The zeta potential decreased when the pH increased from 4 to 10 in the 10 mmol/L NaCl solution (Fig. 4a). The decreased zeta potential was attributed to increased deprotonation of

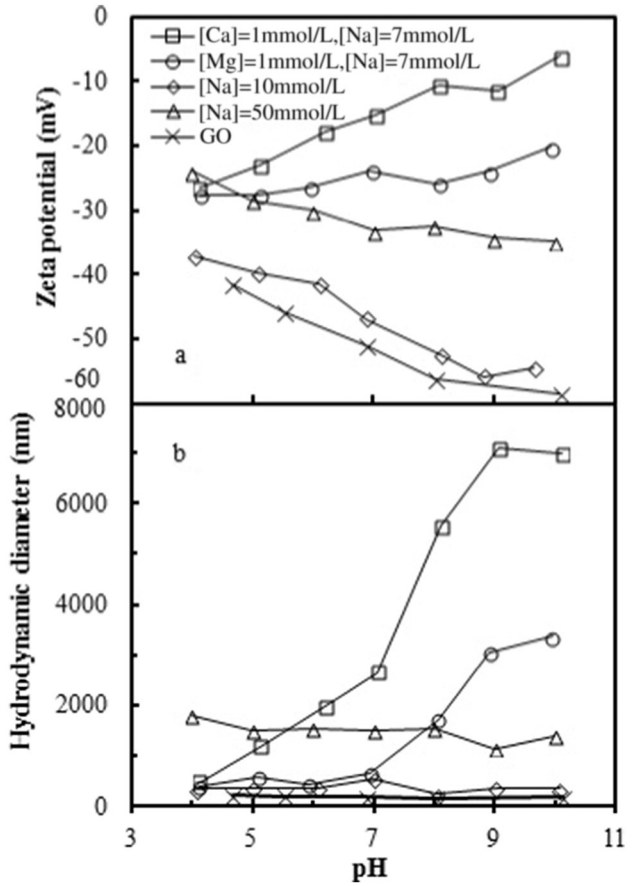

Fig. 4 – (a) Zeta potential and (b) hydrodynamic diameter of GO nanoparticles as a function of final pH in 10 and 50 mmol/L NaCl, 1 mmol/L $CaCl_2$ + 7.0 mmol/L NaCl and 1 mmol/L $MgCl_2$ + 7.0 mmol/L NaCl solutions. GO content = 10 mg/L, ionic strength in the binary component solution = 10 mmol/L.

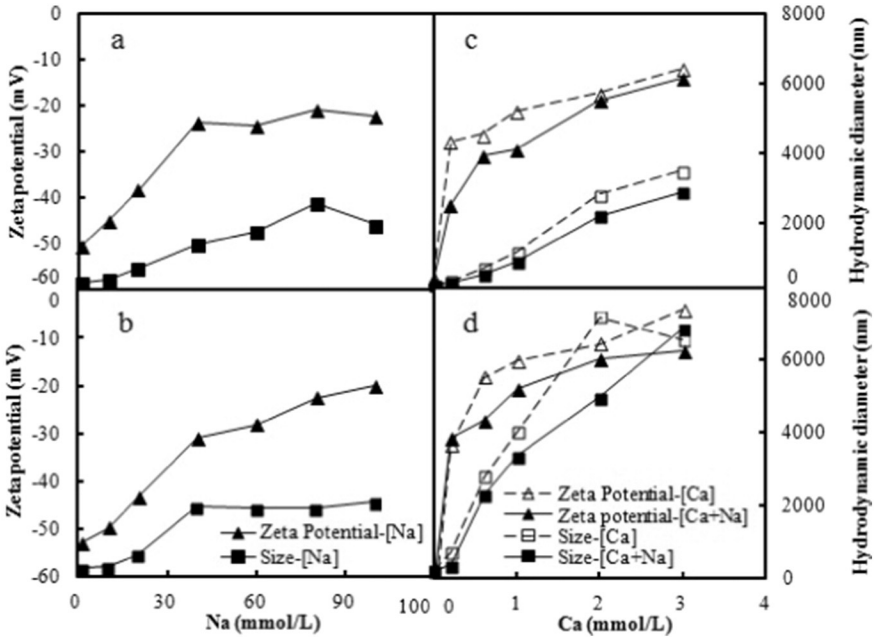

Fig. 5 – Effects of Na^+ concentration on the zeta potential and size of GO nanoparticles at pH = 4.4 ± 0.1(a) and pH = 7.0 ± 0.1 (b); effects of Ca^{2+} concentration, with and without Na^+, on the zeta potential and size of GO nanoparticles at pH = 4.4 ± 0.1(C) and (D) pH = 7.0 ± 0.1. GO content = 10 mg/L, ionic strength in the binary component solution = 10 mmol/L.

the –COOH and –OH groups to form more negatively charged sites, which explains the lower values obtained for the GO without ion addition (Fig. 4a). Deprotonation of the carboxylic groups plays a key role in increasing the GO stability due to surface charge development at increasing pH. In fact, the deprotonation of –OH is much weaker, compared to –COOH, and may not contribute much to the surface charge development on GO (Szabo et al., 2006a; Whitby et al., 2011).

The zeta potential values were higher in the 50 mmol/L solution than in the 10 mmol/L NaCl solution in the entire pH range. The Raman spectroscopic results in Fig. 3 show that Na^+ did not induce significant changes in the GO spectra either in intensity or peak shift; therefore Na^+ does not have strong interaction with the surface functional groups on GO. Thus the increased zeta potential at the high NaCl concentration was attributed to electrostatic attraction due to the presence of more Na^+ into the electrical diffuse layer. According to classical colloidal theory (Russel et al., 1989), more Na^+ will be adsorbed in the diffuse layer to screen the negative surface charge as the electrolyte concentration increases. In the NaCl solutions, the positive charges generated by the Na^+ adsorbed into the diffuse layer were lower than the increased negative charges generated by deprotonation of the functional groups with increasing pH.

In contrast to the decreased zeta potential in the Na^+ solutions with increasing pH, the zeta potential increased in the divalent cation solutions ($Ca^{2+}$and Mg^{2+}), which is consistent with the Ca^{2+} adsorption results (Fig. 1). The results suggest that large amounts of Ca^{2+} were absorbed on the GO surface, which changed the negative carboxyl sites $–COO^-$ to positive sites $–COOCa^+$. The amount of positive charge generated by the adsorbed cations exceeded the increased negative charges formed by the deprotonation of the functional groups with increasing pH. Specific adsorption of cations at higher pH can even reverse the sign of the zeta potential of colloidal particles (Russel et al., 1989). The higher zeta potential values at high pH in the Ca^{2+} + Na^+ with respect to Na^+ and Mg^{2+} + Na^+ solutions suggested that the adsorption of Ca^{2+} was stronger than that of the other cations.

The pH also had different effects on the particle size in the four solutions (Fig. 4b). The Dh in the 10 and 50 mmol/L NaCl solutions was not affected much in the pH range of 4–10. The average Dh of the dispersed GO in the 10 mmol/L NaCl solution was about 360 nm (Fig. 4b), which was similar to the lateral dimensions (*i.e.*, 300–800 nm) of the GO nanosheets. Transmission electron microscopy (TEM) images (Appendix A Fig. S2) show a small piece of GO nanosheet with a length of about 200 nm in the upper-right corner and a large piece with several layers of nanosheets stacked together, with a length of about 750 nm at the center. The GO nanosheets could also undergo some folding, which would affect the measured particle size (Szabó et al., 2006b).

In the Mg^{2+} + Na^+ solution, the Dh increased in the pH range of 7–10. The particle size increase was even more dramatic in the Ca^{2+} + Na^+ solution, and occurred over a broad pH range of 5–10. The Dh of GO nanoparticles was also found to be larger in Ca^{2+} than Mg^{2+} solutions, at pH = 5.5, in the concentration range from 1 to 10 mmol/L (Chowdhury et al., 2013).

The stability of a colloidal suspension is determined by electrostatic repulsion and van der Waals attraction between the charged particles (Szabó et al., 2006b). Zeta potential indicates the degree of the repulsion. When the absolute potential value is high (negative or positive), the repulsion force is higher than the attraction force, which prevents the GO nanoparticles from aggregating. The high negative

potential in the 10 mmol/L NaCl solution prevented the nanoparticles from aggregating in the whole pH range tested. In the Ca^{2+} + Na^{+} and Mg^{2+} + Na^{+} solutions, the increased Dh with increasing pH was coincident with the decreasing absolute value of the zeta potential.

The zeta potential and size of GO nanoparticles at pH 4.4 and 7.0 were also investigated as function of Na^{+} and Ca^{2+} concentrations (Fig. 5). The zeta potential increased with increasing Na^{+} concentration from zero to 40 mmol/L at pH 4.4 and up to 110 mmol/L at pH 7. These results are consistent with the pH-dependent stability behavior of functionalized fullerene (nC60) and carbon nanotubes in NaCl solution (Bouchard et al., 2009; Li and Huang, 2010; Chowdhury et al., 2012).

The Dh increased gradually with Na^{+} concentration from about 350 to 2000 nm for both pH values (Fig. 5a-b). Appendix A Fig. S4 shows a TEM image of the loose GO flocs formed in a 100 mmol/L NaCl solution. The solid particles in the image are NaCl precipitates formed after the suspension sample was dried for TEM analysis. Lanphere and coworkers in 2014 reported that the GO nanoparticles formed aggregates when the KCl concentration was higher than 32 mmol/L (Lanphere et al., 2014).

The effect of Ca^{2+} concentration on the zeta potential and size of GO nanoparticles at different pH is presented in Fig. 5c–d. The zeta potential and Dh of the GO nanoparticles were also measured in the binary component solution, Ca^{2+}+Na^{+}, at 10 mmol/L constant ionic strength. The zeta potential increased with increasing Ca^{2+} concentration more dramatically at pH 7 than at pH 4.4. The Dh did not increase much when the Ca^{2+} concentration increased from 0 to 1 mmol/L at pH = 4.4, but it started to increase at 0.2 mmol/L of Ca^{2+} at pH = 7. The particle size increased from ~400 nm to ~6900 nm with increasing Ca^{2+} concentration from 0.2 to 3 mmol/L. The results indicated that the aggregation effect of Ca^{2+} on GO was more significant at higher pH level, which is consistent with high adsorption of Ca^{2+} at higher pH (Fig. 1). TEM images (Appendix A Fig. S3) showed that dense GO flocs formed in a 2 mmol/L $CaCl_2$ solution. Fig. 5c–d also show that the presence of Na^{+} in the $CaCl_2$ solutions decreased the zeta potential of GO, which agrees with the decrease in Ca^{2+} adsorption caused by Na^{+} (Figs. 1 and 2). In addition to the chemical adsorption of Ca^{2+} at the GO surface, some Ca^{2+} cations could be adsorbed into the diffused layer through electrostatic attraction. High Na^{+} concentration could decrease the amount of Ca^{2+} in the diffuse layer, thus reducing the adsorption of Ca^{2+}. However, Na^{+} should not decrease the amount of chemically adsorbed Ca^{2+}.

3. Conclusions

GO had high adsorption capacity for Ca^{2+} when pH was greater than 7, while it had very low adsorption for Na^{+}. Ca^{2+} adsorption dramatically changed the Raman spectra of GO, while Na^{+} adsorption had no effect on the Raman spectra. Raman spectroscopy showed that Ca^{2+} ions were strongly adsorbed on the GO surface with dramatic changes in the typical GO spectra. The zeta potential of GO decreased with increasing pH in the NaCl solution due to increased deprotonation of the carboxyl and hydroxyl groups on GO. The zeta potential increased with increasing pH in the Ca^{2+} solution instead, because of the formation of the positive sites –$COOCa^{+}$. As a result, the GO suspension was more stable in NaCl solutions, while GO nano sheets formed aggregates in $CaCl_2$ solutions when the pH increased from 4 to 9. The results of this study show that Ca^{2+} has strong interaction with the surface functional group of GO which suggest formation of inner-sphere complex.

Appendix A. Supplementary data

Supplementary data to this article can be found online at http://dx.doi.org/10.1016/j.jes.2017.01.008.

REFERENCES

Arvidsson, R., Molander, S., Sanden, A.B., 2013. Review of potential environmental and health risks of the nanomaterial graphene. Hum. Ecol. Risk. Assess. 19, 873–887.

Balandin, A.A., Ghosh, G., Bao, W., Calizo, I., Teweldebrhan, D., Miao, F., Lau, C.N., 2008. Superior thermal conductivity of single-layer graphene. Nano Lett. 8 (3), 902–907.

Bouchard, D., Ma, X., Isaacson, C., 2009. Colloidal properties of aqueous fullerenes: isoelectric points and aggregation kinetics of C_{60} and C_{60} derivatives. Environ. Sci. Technol. 43, 6597–6603.

Cañamares, M.V., Lombardi, J.R., 2015. Raman, SERS, and DFT of mauve dye: adsorption on Ag nanoparticles. J. Phys. Chem. C 119 (25), 14297–14303.

Chandra, V., Park, J., Chun, Y., Lee, J.W., Hwang, I.C., Kim, K.S., 2010. Water-dispersible magnetite-reduced graphene oxide composites for arsenic removal. ACS Nano 4 (7), 3979–3986.

Chen, L., Hu, P., Zhang, L., Huang, S., Luo, L., Huang, C., 2012. Toxicity of graphene oxide and multi-walled carbon nanotubes against human cells and zebrafish. Sci. China 55 (10), 2209–2216.

Chowdhury, I., Duch, M.C., Gits, C.C., Hersam, M.C., Walker, S.L., 2012. Impact of synthesis methods on the transport of single walled carbon nanotubes in the aquatic environment. Environ. Sci. Technol. 46 (21), 11752–11760.

Chowdhury, I., Duch, M.C., Mansukhani, N.D., Hersam, M.C., Bouchard, D., 2013. Colloidal properties and stability of graphene oxide nanomaterials in the aquatic environment. Environ. Sci. Technol. 47, 6288–6296.

Chowdhury, I., Duch, M.C., Mansukhani, N.D., Hersam, M.C., Bouchard, D., 2014. Deposition and release of graphene oxide nanomaterials using a quartz crystal microbalance. Environ. Sci. Technol. 48 (2), 961–969.

Das, B., Voggu, R., Rout, C.S., Rao, C.N.R., 2000. Changes in the electronic structure and properties of graphene induced by molecular charge-transfer. Chem. Commun. (41), 5155–5157.

Dreyer, D., Park, S., Bielawski, C.W., Ruoff, R.S., 2010. The chemistry of graphene oxide. Chem. Soc. Rev. 39 (1), 228–240.

Emara, M., Farid, N.A., Wasfi, A.M., Bahr, M.M., Abd-Elbary, H.M., 1984. Thermodynamics of ion-association in aqueous solutions of calcium and magnesium substituted hydroxybenzoates using an ion-selective electrode technique. J. Phys. Chem. 88, 3345–3348.

Feriancikova, L., Xu, S., 2012. Deposition and remobilization of graphene oxide within saturated sand packs. J. Hazard. Mater. 235-236 (5), 194–200.
Ferrari, A.C., Robertson, J., 2000. Interpretation of Raman spectra of disordered and amorphous carbon. Phys. Rev. B 61 (20), 14095.
Gu, D., Fein, J.B., 2015. Adsorption of metals onto graphene oxide: surface complexation modeling and linear free energy relationships. Colloids Surf. A Physicochem. Eng. Asp. 481, 319–327.
Guo, J., Wang, R., Tjiu, W.W., Pan, J., Liu, T., 2012. Synthesis of Fe nanoparticles@graphene composites for environmental applications. J. Hazard. Mater. 225-226, 63–73.
Hem, J.D., 1992. Study and interpretation of chemical characteristics of natural water. 3d ed.U.S. Geological Survey Water-Supply Paper 2254, p. 263.
Lanphere, J.D., Luth, C.J., Walker, S.L., 2013. Effects of solution chemistry on the transport of graphene oxide in saturated porous media. Environ. Sci. Technol. 47 (9), 4255–4261.
Lanphere, J.D., Rogers, B., Luth, C.J., Bolster, C.H., Walker, S.L., 2014. Stability and transport of graphene oxide nanoparticle in groundwater and surface water. Environ. Eng. Sci. 31 (7), 350–359.
Lee, C., Wei, X., Kysar, J.W., Hone, J., 2008. Measurement of the elastic properties and intrinsic strength of monolayer graphene. Science 321 (18), 385–388.
Lee, D.W., De Los Santos, V.L., Seo, J.W., Leon Felix, L., Bustamante, D.A., Cole, J.M., Barnes, C.H.W., 2010. The structure of graphite oxide: investigation of its surface chemical groups. J. Phys. Chem. B 114, 5723–5728.
Lerf, A., He, H., Forster, M., Klinowski, J., 1998. Structure of graphite oxide revisited. J. Phys. Chem. B 102, 4477–4482.
Li, M.H., Huang, C.P., 2010. Stability of oxidized single-walled carbon nanotubes in the presence of simple electrolytes and humic acid. Carbon 48, 4527–4534.
Li, Y., Zhang, P., Du, Q., Peng, X., Liu, T., Wang, Z., Xia, Y., Zhang, W., Wang, K., Zhu, H., Wu, D., 2011. Adsorption of fluoride from aqueous solution by graphene. J. Colloid Interface Sci. 363, 348–354.
Li, B., Yang, J., Huang, Q., Zhang, Y., Peng, C., Zhang, Y., He, Y., Shi, J., Li, W., Hu, J., Fan, C., 2013. Biodistribution and pulmonary toxicity of intratracheally instilled graphene oxide in mice. NPG Asia Mater. 5 (e44), 1–8.
Liu, W., Zhao, X., Wang, T., Zhao, D., Ni, J., 2016. Adsorption of U (VI) by multilayer titanate nanotubes: effects of inorganic cations, carbonate and natural organic matter. Chem. Eng. J. 286, 427–435.
Luo, X., Wang, C., Luo, S., Dong, R., Tu, X., Zeng, G., 2012. Adsorption of As(III) and As(V) from water using magnetite Fe_3O_4–reduced graphite oxide–MnO_2 nanocomposites. Chem. Eng. J. 187, 45–52.
National Academy of Sciences, 1977. Drinking Water and Health. National Academy Press, Washington, DC, pp. 400–411.
Niyogi, S., Bekyarova, E., Itkis, M.E., McWilliams, J.L., Hamon, M.A., Haddon, R.C., 2006. Solution properties of graphite and graphene. J. Am. Chem. Soc. 128, 7720–7721.
Ouatmane, A., Hafidi, M., Gharous, M.E., Revel, J.C., 1999. Complexation of calcium ions by humic and fulvic acid. Analusis 27, 428–437.
Park, S., Ruoff, R.S., 2009. Chemical methods for the production of graphene. Nat. Nanotechnol. 2009 (4), 217–224.
Pei, Z., Li, L., Sun, L., Zhang, S., Shan, X., Yang, S., Wen, B., 2013. Adsorption characteristics of 1,2,4-trichlorobenzene, 2,4,6-trichlorophenol, 2-naphthol and naphthalene on graphene and graphene oxide. Carbon 51, 156–163.
Ramesha, G.K., Kumara, A.V., Muralidhara, H.B., Sampath, S., 2011. Graphene and graphene oxide as effective adsorbents toward anionic and cationic dyes. J. Colloid Interface Sci. 361 (1), 270–277.
Rao, C.N.R., Sood, A.K., Subrahmanyam, K.S., Govindaraj, A., 2009. Graphene: the new two-dimensional nanomaterial. Angew. Chem. Int. Ed. 48, 7752–7777.
Russel, W.B., Saville, D.A., Schowalter, W.R., 1989. Colloidal Dispersions. Cambridge University Press, New York.
Schinwald, A., Murphy, F.A., Jones, A., MacNee, W., Donaldson, K., 2012. Graphene-based nanoplatelets: a new risk to the respiratory system as a consequence of their unusual aerodynamic properties. ACS Nano 6 (1), 736–746.
Singh, V., Joung, D., Zhai, L., Das, S., 2011a. Graphene based materials: past, present and future. Prog. Mater. Sci. 56, 1178–1271.
Singh, S.K., Singh, M.K., Nayak, M.K., Kumari, S., Shrivastava, S., Gracio, J.J.A., Dash, D., 2011b. Thrombus inducing property of atomically thin graphene oxide sheets. ACS Nano 5, 4987–4996.
Sitko, R., Turek, E., Zawisza, B., Malicka, E., Talik, E., Heimann, J., Gagor, A., Feista, B., Wrzalikb, R., 2013. Adsorption of divalent metal ions from aqueous solutions using graphene oxide. Dalton Trans. 42, 5682–5689.
Sposito, G., 2008. The Chemistry of Soils. second ed. Oxford University Press, New York.
Stankovich, S., Piner, R.D., Nguyen, S.T., Ruoff, R.S., 2006. Synthesis and exfoliation of isocyanate-treated graphene oxide nanoplatelets. Carbon 44, 3342–3347.
Stumm, W., 1992. Chemistry of the Solid-Water Interface. Wiley-Interscience Publication, New York, p. 24.
Szabo, T., Tombacz, E., Illes, E., Dekany, I., 2006a. Enhanced acidity and pH-dependent surface charge characterization of successively oxidized graphite oxides. Carbon 44, 537–545.
Szabó, T., Berkesi, O., Forgó, P., Josepovits, K., Sanakis, Y., Petridis, D., Dékány, I., 2006b. Evolution of surface functional groups in a series of progressively oxidized graphite oxides. Chem. Mater. 18 (11), 2740–2749.
Tan, P., Sun, J., Hu, Y., Fang, Z., Bi, Q., Chen, Y., Cheng, J., 2015. Adsorption of Cu, Cd, and Ni from aqueous single metal solutions on graphene oxide membranes. J. Hazard. Mater. 297, 251–260.
Voggu, R., Das, B., Rout, C.S., Rao, C.N.R., 2008. Effects of charge transfer interaction of graphene with electron donor and acceptor molecules examined using Raman spectroscopy and cognate techniques. J. Phys.: Condens. Matter 20 (47), 472204.
Wang, H., Yuan, X., Wu, Y., Huang, H., Zeng, G., Liu, Y., Wang, X., Lin, N., Qi, Y., 2013. Role of graphene/metal oxide composites as photocatalysts, adsorbents and disinfectants in water treatment: a review. Appl. Surf. Sci. 279-432.
Whitby, R.L.D., Korobeinyk, A., Gun'ko, V.M., Busquets, R., Cundy, A.B., Laszlo, K., Skubiszewska-Zieba, J., Leboda, R., Tombacz, E., Toth, I.Y., Kovacs, K., Mikhalovsky, S.V., 2011. pH-driven physicochemical conformational changes of single-layer graphene oxide. Chem. Commun. 47, 9645–9647.
Xu, Y., Hong, W., Bai, H., Li, C., Shi, G., 2009. Strong and ductile poly(vinyl alcohol)/graphene oxide composite films with a layered structure. Carbon 47, 3538–3543.
Yang, S.T., Chang, Y.L., Wang, H.F., Liu, G.B., Chen, S., Wang, Y.W., Liu, Y.F., Cao, A.N., 2010. Folding/aggregation of graphene oxide and its application in Cu^{2+} removal. J. Colloid Interface Sci. 35, 122–127.
Zhao, G., Li, J., Ren, X., Chen, C., Wang, X., 2011a. Few-layered graphene oxide nanosheets as superior sorbents for heavy metal ion pollution management. Environ. Sci. Technol. 45, 10454–10462.
Zhao, G., Ren, X., Gao, X., Tan, X., Li, J., Chen, C., Huang, Y., Wang, X., 2011b. Removal of Pb(II) ions from aqueous solutions on few-layered graphene oxide nanosheets. Dalton Trans. 40, 10945–10952.
Zhao, J., Wang, Z., White, C.J., Xing, B., 2014. Graphene in the aquatic environment: adsorption, dispersion, toxicity and transportation. Environ. Sci. Technol. 48, 9995–10009.